



Article

Adhesion Energy for Nonideal Cantilever and Its Relation to Casimir–Lifshitz Forces

Ivan A. Soldatenkov ¹  and Vitaly B. Svetovoy ^{2,*} 

¹ Ishlinsky Institute for Problems in Mechanics, Russian Academy of Sciences, Prospect Vernadskogo 101-1, Moscow 119526, Russia; iasoldat@hotmail.com

² A. N. Frumkin Institute of Physical Chemistry and Electrochemistry, Russian Academy of Sciences, Leninsky Prospect 31 Bld. 4, Moscow 119071, Russia

* Correspondence: svetovoy@yandex.ru

Abstract: The method of the adhered cantilever, borrowed from microtechnology, can help in gaining fundamental knowledge about dispersion forces acting at distances of about 10 nm, which are problematic to access in the usual Casimir-type experiments. A recently presented setup measures the shape of cantilevers with high precision, which is needed for analyzing the involved forces. The first measurements reveal several nonidealities crucial for the data analysis. In this paper, a generalized formula is deduced that relates the parameters of a cantilever to the adhesion energy. The application of the formula is demonstrated using the first test result from the setup, where a silicon cantilever adhered to a substrate sputters with ruthenium. Detailed information of the roughness of interacting surfaces, which deviates significantly from the normal distribution, is emphasized. Although not crucial, the electrostatic contribution can be significant due to the slight twisting of the cantilever. The theoretical prediction of the adhesion energy is based on Lifshitz theory. Comparing theory and experiment yields a contact distance of 45 nm and an adhesion energy of 1.3 $\mu\text{J}/\text{m}^2$, resulting from the Casimir–Lifshitz forces. Significant uncertainties arise from the uncontrolled electrostatic contribution. Factors that need to be addressed to measure weak adhesion between rough surfaces are highlighted.

Keywords: Casimir–Lifshitz forces; adhered cantilever; adhesion energy; forces at short distances; surface roughness



Citation: Soldatenkov, I.A.;

Svetovoy, V.B. Adhesion Energy for Nonideal Cantilever and Its Relation to Casimir–Lifshitz Forces. *Physics* 2024, 6, 1204–1221. <https://doi.org/10.3390/physics6040074>

Received: 14 August 2024

Revised: 27 September 2024

Accepted: 15 October 2024

Published: 23 October 2024



Copyright: © 2024 by the authors. Licensee MDPI, Basel, Switzerland. This article is an open access article distributed under the terms and conditions of the Creative Commons Attribution (CC BY) license (<https://creativecommons.org/licenses/by/4.0/>).

1. Introduction

Casimir–Lifshitz forces [1–3] are omnipresent because they originate from the quantum (and thermal) fluctuations of the electromagnetic field, which cannot be turned off. These forces begin to act at separation distances around $h = 100$ nm [4–6], where the forces have been precisely measured between 3D (three-dimensional) objects [7–12]. These forces depend on the distance as $h^{-\alpha}$, with the exponent α spanning 3 to 4 [3]. Near the lower limit, the retardation effect can be neglected, but near the upper limit, it must be fully considered. Historically, forces near the lower limit have been called van der Waals forces [13]. However, here, the term “dispersion forces” (DFs) is used to refer to these fluctuation-induced forces at all separation distances. Although forces decrease rapidly at distances greater than 100 nm, several measurements have been successful even at distances exceeding 1 μm [14,15]. In contrast, only a few measurements have been made at short separations below 50 nm [16–19], and the precision of these measurements has been relatively low. Two major factors complicate measurements at close distances [6]. First, when the distance between objects is quite small, systems with elastic suspensions, such as the cantilever in an atomic force microscope (AFM) [8] or the torsional rod [9,10], can lose stability and cause objects to jump into contact. Second, the gap between objects can only be measured with limited precision, typically of the order of 1 nm. Therefore, the closer the objects are, the greater the effective uncertainty in the measured force.

Casimir–Lifshitz forces begin to play a significant role in modern microelectromechanical systems (MEMSs) [6,20–24], as the distances involved are quite small, but the area of interaction is large. Therefore, it is not surprising that these forces are measured using various types of MEMS devices. Recently, a new method has been proposed [25] for simultaneously measuring the force and adhesion energy at small distances. This method does not suffer from instability at small separations between objects. The method originates from the stiction problem in MEMS manufacturing [26–31]. The final step in the fabrication process involves rinsing. As the liquid dries, strong capillary forces draw the soft elements of the MEMS together. After complete drying, the elements remain locked [32,33]. The cause of this adhesion is the unavoidable dispersion interaction between the surfaces that are in contact. Stiction can occur not only during the fabrication but also during the operation of the device, resulting in device malfunction. The issue of stiction has received great attention because of its high practical significance [34,35].

The so-called “adhered cantilever” (see Figure 1) has been used as a model system to investigate the stiction phenomenon [26,32,33,33,34,36–39]. This is an elastic beam that has one end fixed at a certain height above a substrate, and the other end is adhered to the substrate. The length of the unadhered part of the beam provides information about the adhesion energy per unit area between the beam and the substrate at the adhered location [36,40]. On the other hand, the precise shape of the adhered cantilever depends on the forces acting on it outside of the adhered area. The intentional application of the electrostatic forces to the cantilever outside the adhesion region has been discussed [37], and the influence of the DF near the adhered end on the shape of the cantilever has been demonstrated [41] on a measurable level. Microfabricated surfaces always have some level of roughness, so the contacting surfaces are separated by an average distance h_0 , at which the attractive forces are balanced by the repulsive forces from the elastic deformation of the asperities. Outside the adhered area, the attractive forces also operate, but they are balanced by the additional bending of the beam, which contributes to the overall shape of the cantilever. The adhered cantilever remains in equilibrium and maintains its stability at any given distance h_0 . However, forces acting between the beam and the substrate can cause the unadhered length s to change.

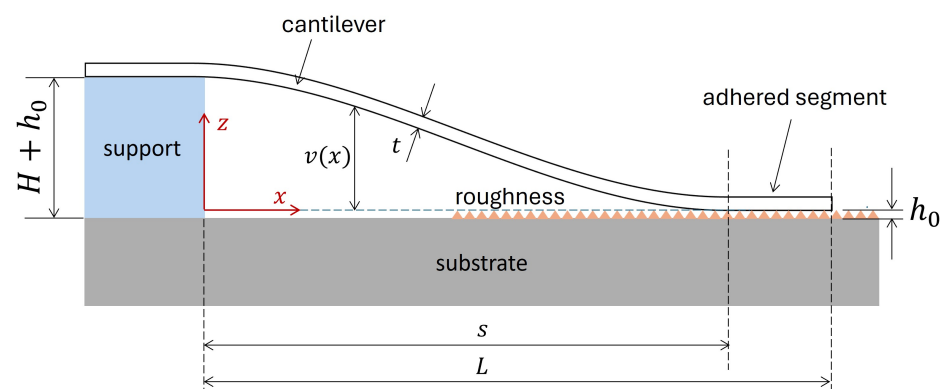


Figure 1. Schematic view of the adhered cantilever. The average contact distance due to roughness is h_0 , and the height of the cantilever above the substrate is $h_0 + v(x)$. The choice of the coordinate system is shown, where the y -axis runs along the width of the cantilever.

Thus, the adhered cantilever can be used to measure the adhesion energy simultaneously with the DF acting near the adhered end, as was proposed in a new experiment [25]. To obtain the necessary information, one has to precisely measure the shape of the adhered cantilever. In this paper, the DFs outside of the adhered area are discussed only briefly, since more experimental and theoretical efforts are needed to separate the DFs against the background (electrostatics and nonidealities of the cantilever). The main focus here is on the adhesion energy. This energy is defined as the work per unit area required to detach and separate two surfaces over an infinite distance. In the case of the adhered cantilever,

this energy is related to the geometrical and mechanical characteristics of the cantilever as follows [36,40]:

$$\Gamma_0 = \frac{3Et^3H^2}{2s^4}, \quad (1)$$

where E is Young's modulus of the beam material, t is the thickness of the beam, and H is the height of the fixed end above the substrate. The classic shape of a cantilever, by definition, is understood as the shape when no external forces are applied to the cantilever in the unadhered region. Dispersion forces, which operate close enough to the adhered region, provide a deviation from the classic shape on a 1% level and can be neglected in the calculation of the adhesion energy in the first approximation. The classic shape, represented by the gap $v(x)$ (see Figure 1), is described by the following function:

$$v(x) = H \begin{cases} 2(x/s)^3 - 3(x/s)^2 + 1, & x \leq s, \\ 0, & x > s. \end{cases} \quad (2)$$

Originally, it was proposed to measure the shape of the adhered cantilever using interferometric methods [36,40]. In the most advanced experiment [20], the adhesion energy between the micromachined surfaces of polysilicon and silicon was measured. Although the errors in the measured Γ_0 were significant, it was still possible to establish a correlation between the measured values and the van der Waals forces.

An advanced interferometric system [42] based on the Nomarski differential interference contrast method [43] has been recently presented. This system scans along the cantilever to determine its shape with a precision of 1 nm in the range of heights up to 10 μm . The minicantilevers used in this system are fabricated using microtechnology methods. They have a length of 12 mm, a width of 200 μm , and a thickness of 10 μm . These dimensions are one order of magnitude larger in all three directions than in a previous similar system [20].

The first measurements revealed deviations in the cantilever from the ideal case. In particular, the beam at the fixed end was always tilted at an angle relative to the substrate. This effect, previously observed for microcantilevers and attributed to the finite compliance of the beam support [44], is now believed to be caused by the presence of external particles between the substrate and the wafer containing the cantilever. Additionally, longer cantilevers may be slightly twisted, with one side adhering to the substrate and the other hanging over it. Due to their length and thickness, compared to microcantilevers, gravity can influence both the shape and the measured value of the adhesion energy of these cantilevers.

In this paper, it is shown that the observed nonidealities are significant for analysing minicantilevers. A new expression for the adhesion energy is derived. One specific set of data from Ref. [42] is used to demonstrate how the adhered cantilever method can be applied to obtain information on the DF acting between the cantilever and the substrate in the adhered area.

2. Adhered Cantilever

2.1. Ideal Case

Figure 1 shows a cantilever with a length L , thickness t , width w , and an unadhered segment of length s . The adhered segment is parallel to the substrate and has an equilibrium distance of h_0 , which is not known a priori. The roughness of the contacting surfaces determines this distance, and gravity is assumed to have a negligible effect. Various theories are used to calculate this equilibrium distance under the influence of the DF [24,45–47]. These theories differ mainly in how they treat roughness, forces, and material plasticity. It is assumed that the cantilever is parallel to the substrate at its fixed end and subjected to no external forces. The shape of the cantilever obeys an equation from elasticity theory:

$$\frac{d^4v}{dx^4} = 0. \quad (3)$$

Equation (3) needs to be solved with the following boundary conditions:

$$v(0) = H, v'(0) = 0; v(s) = 0, v'(s) = 0, \tag{4}$$

where the prime indicates the x -derivative. The solution to this problem is given by Equation (2).

The adhesion energy per unit area Γ can be found (see, e.g., [36]) by minimizing the total energy of the adhered cantilever with respect to s . The total energy is

$$E_{\text{tot}} = U(s) - \Gamma w(L - s), \tag{5}$$

where w denotes the width of the cantilever. The first term $U(s)$ in Equation (5) is the elastic energy of the deformed part of the beam, and the second term is the surface energy. The elastic energy as a functional of the shape of the cantilever is expressed as

$$U(s) = \frac{wD}{2} \int_0^s dx \left(\frac{d^2v}{dx^2} \right)^2, \quad D = \frac{Et^3}{12} \tag{6}$$

where D is the flexural rigidity. The minimization of the total energy (5) in s results in $\Gamma = \Gamma_0$, where Γ_0 is given by Equation (1).

2.2. Shape of the Minicantilever in a Realistic Case

2.2.1. Nonzero Gravity and Slope

In contrast to microcantilevers used for the analysis of adhesion in MEMSs [20,34,37], where planar microtechnology has been used, the minicantilevers designed for measurements of the DF [25,42] are fabricated in a different process. First, the cantilevers are produced from silicon-on-insulator (SOI) wafer, where the top Si layer, 10 μm thick, is separated from the base Si by a thin (1 μm) SiO_2 layer. The bearing plate is an ordinary Si wafer on which a separating layer with a nominal thickness of 5 μm is spin-coated and patterned by photolithography. The measuring chip consists of a stack of two wafers, one with cantilevers and one with a bearing plate, as shown schematically in Figure 2.

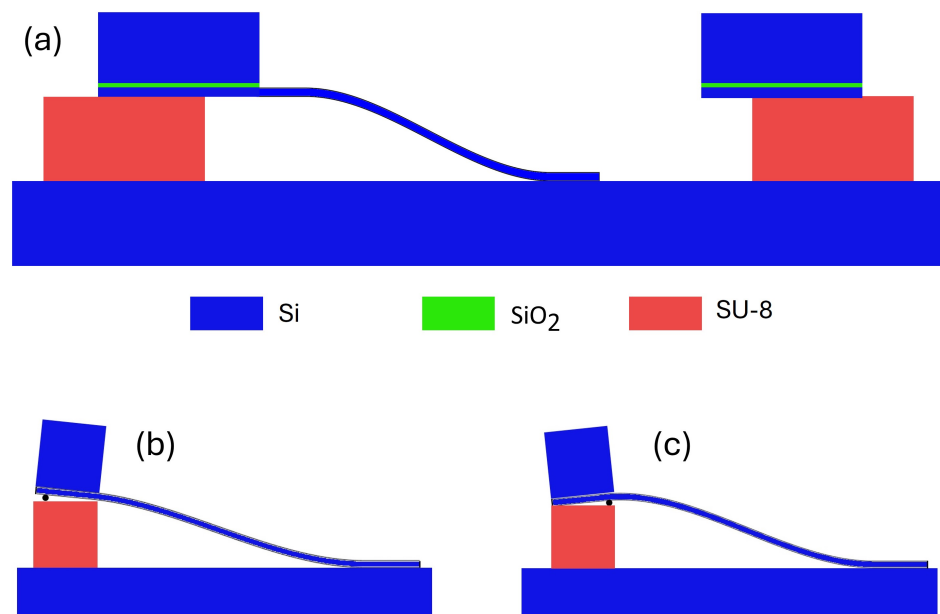


Figure 2. (a) Cross-section of the measuring chip. The SOI wafer with cantilevers is placed on top of the bearing wafer that contains a separating SU-8 layer. (b) Negative slope at the fixed end due to an external particle between the wafers. (c) Positive slope due to a particle.

In the ideal case, the two wafers are completely parallel to each other, and the slope of the cantilever at the fixed end is zero. However, the area of contact between the SOI wafer and the separating layer is estimated as 123 mm² (the exact dimensions of the chip are presented in Ref. [42]). In this large area, it is complicated to exclude a dust particle between the wafers. Such a particle may result in a nonzero slope of the fixed end of the cantilever with respect to the bearing substrate. Given the particle position, the slope can be negative or positive, as shown in Figure 2b,c. This is realized as demonstrated in Ref. [42]. Therefore, one has to modify boundary condition (4) at $x = 0$ as follows:

$$v(0) = H, \quad v'(0) = \vartheta, \tag{7}$$

where $|\vartheta| \ll 1$ is the angle of the slope. The height H is also an a priori parameter that has to be found from the measured shape of the cantilever $v(x)$ because the nominal thickness of the SU-8 layer does not coincide with the exact height. Interestingly, in planar microtechnology, the same mechanism for the slope formation is not possible and, nevertheless, the slope exists in this case too due to finite compliance of the support [37,44].

An additional difference between micro- and minicantilevers is related to the influence of gravity, which can be neglected in the case of microcantilevers but not in the case of minicantilevers. As a result, the equation describing the shape of the cantilever now reads:

$$D \frac{d^4 v}{dx^4} = -\rho g t, \tag{8}$$

where ρ is the mass density of the beam material, and g is the free-fall acceleration. Therefore, the gravity contributes to the shape $v(x)$. By introducing normalized variables

$$\xi = x/s, \quad \zeta(\xi) = v(x)/H, \tag{9}$$

and normalized parameters

$$a = \frac{\vartheta s}{H}, \quad \gamma = \frac{\rho g s^4}{2Et^2 H} > 0, \tag{10}$$

one finds the solution of Equation (8) under boundary condition (7) as follows:

$$\zeta(\xi) = -\gamma \xi^4 + A_3 \xi^3 + A_2 \xi^2 + A_1 \xi + 1, \tag{11}$$

where

$$A_3 = 2 + a + 2\gamma, \quad A_2 = -3 - 2a - \gamma, \quad A_1 = a. \tag{12}$$

Let us note that in the experimental conditions [42], $a \sim 1$ and $\gamma \sim 1$.

2.2.2. Factor of Twisting

The first experiments with adhered minicantilevers revealed an additional deviation from the ideal case [42]. It was found that the beam is slightly twisted along its length as the cross-section in Figure 3, right, shows. Due to the twisting, the adhered end is not exactly parallel to the substrate. In this area, one side of the beam, for example, the left side, is in direct contact with the substrate, but the other side hangs above the substrate at a certain height. Thus, the adhered part of the cantilever is tilted to some angle φ in the direction of the y -axis (along the width of the beam). The gap $v(x, y)$ is now a function of two variables, but since the twisting is relatively small, the dependence of $\varphi(x)$ on x is assumed to be linear. Let $v(x)$ describe the left edge of the beam; then, $v(x, y) = v(x) + \varphi(x)(w/2 + y)$, where y changes in the range $-w/2 \leq y \leq w/2$. At $x = 0$ and $x = s$, one has $\varphi(0) = 0$ and $\varphi(s) = \Delta v/w$, and the transition between these two values is linear in x . Here, Δv is the absolute value of the height difference between the left and right wings of the cantilever at

$x = s$. This value can be directly measured interferometrically. Therefore, for $0 \leq x \leq s$, one finds:

$$v(x, y) = v(x) + \Delta v \left(\frac{x}{s} \right) \left(\frac{1}{2} + \frac{y}{w} \right). \tag{13}$$

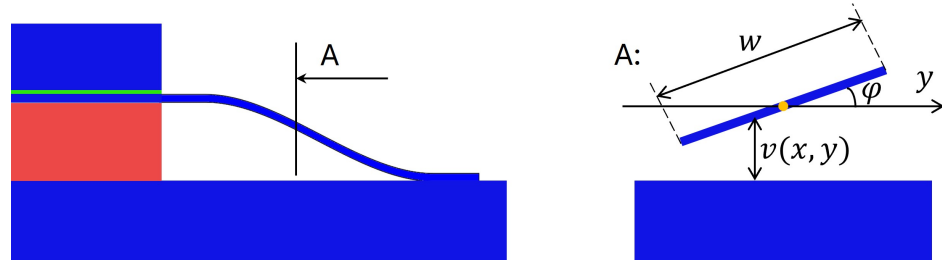


Figure 3. Left: adhered cantilever with the indicated position of the cross-section. Right: cross-section where $v(x, y)$ is the gap.

The second term in Equation (13) is related to the twisting of the cantilever. The experiment, as shown in Section 4.1 below, demonstrates that the linear dependence of the twisting term on x continues close to the point of adhesion $x = s$. In this case, the boundary conditions for the function $v(x, y)$ can be obtained from Equation (13):

$$\begin{aligned} v(0, y) &= H, \quad v'(0, y) = \vartheta + \frac{\Delta v}{s} \left(\frac{1}{2} + \frac{y}{w} \right); \\ v(s, y) &= \Delta v \left(\frac{1}{2} + \frac{y}{w} \right), \quad v'(s, y) = \frac{\Delta v}{s} \left(\frac{1}{2} + \frac{y}{w} \right). \end{aligned} \tag{14}$$

where ϑ is the slope of the left edge of the cantilever. In the normalized form, the twisting changes only the coefficients A_1 in Equation (11), which becomes now a function of the normalized variable $\eta = y/w$:

$$A_1 = a + b(1/2 + \eta), \quad b = \Delta v/H, \tag{15}$$

where b is an additional parameter with a typical value $b \sim 10^{-2}$. In the conditions of the experiment, the angle ϑ is typically $10^{-3} - 10^{-4}$, while the ratio $\Delta v/s$ that characterizes the correction to the beam slope is in the order of 10^{-5} . Therefore, the twisting only slightly disturbs the derivative, but is essential for the function $v(x, y)$.

2.3. Adhesion Energy

2.3.1. General Formula

In the gravitational field, an additional contribution appears in the energy of the deformed beam. Instead of using Equation (6) to model the energy, the energy is as follows:

$$U(s) = \int_{w/2}^{w/2} dy \int_0^s dx \left[\frac{D}{2} \left(\frac{d^2v}{dx^2} \right)^2 + \rho g t v \right]. \tag{16}$$

Here, the second term in square brackets is the potential energy of the deformed beam in the gravitational field if the zero potential is taken at $z = 0$. The minimization of the total energy (5) on s provides the expression for the adhesion energy:

$$\Gamma = -\frac{1}{w} \frac{dU}{ds}. \tag{17}$$

The energy $U(s)$ can be calculated using the shape function $v(x, y)$ defined by Equation (11) with the y -dependent coefficient A_1 (15).

To simplify the analysis, consider first the case of $b = 0$ (no twisting). Calculating the energy $U(s)$ with $v(x)$, one can find the expression for Γ after lengthy algebra. The final result is, however, rather compact:

$$\Gamma = \Gamma_0 \left(1 - \frac{\gamma - a}{3} \right)^2. \tag{18}$$

This result needs to be understood. When $\gamma - a = 0$, the adhesion energy is equal to Γ_0 . With the increase in this parameter, Γ decreases and becomes zero at $\gamma - a = 3$. This is because gravity and a negative slope both cause the beam to approach the substrate, regardless of the forces acting in the adhered area. As the parameter $\gamma - a > 3$ increases further, the adhesion energy increases again, but this region cannot be reached in a realistic system. To see this, let us present the normalized shape (11) in the equivalent form:

$$\zeta(\xi) = -(1 - \xi)^2 \left[\gamma \xi^2 - (2 + a)\xi - 1 \right] \tag{19}$$

where the factor $(1 - \xi)^2$ reflects the boundary conditions at $\xi = 1$. The polynomial in square brackets can have a root within the interval $0 < \xi < 1$. This root appears when $\gamma - a > 3$, and its existence means that the gap becomes negative inside the interval $0 < \xi < 1$. Any physical solution cannot go below the stiff substrate. This means that the lengths s that can be realized must satisfy the condition $\gamma - a < 3$.

In the case of nonzero twisting ($b \neq 0$), the expression for Γ has the following form:

$$\Gamma = \Gamma_0 \left[\left(1 - \frac{\gamma - a}{3} \right)^2 - \frac{\gamma b}{3} \right]. \tag{20}$$

Since $b = \Delta v/H$ is always small in comparison with a and γ , the term with b is the correction made to the main result (18).

2.3.2. Universality of the Solution

The initial assumptions about the adhered cantilever do not include whatever nonzero slope at the fixed end. The expressions (1) for the adhesion energy and (2) for the shape also do not contain the slope [37]. However, the experimental circumstances may differ significantly from the ideal case, as Figures 2 and 3 illustrate. In real-world conditions, the fixed end may hang above the support, and the actual point of support may be in a completely different location. Now, the following question arises: whether the expressions (11) for the shape and (18) or (20) for the adhesion energy are applicable for all possible configurations.

The cantilever is firmly fixed to the base layer of the SOI wafer. The contact with the supporting SU-8 layer can be compliant, but it is not significant since the height is determined experimentally. The most general case is shown in Figure 4. One can imagine three different situations when the information on the shape of the cantilever is collected starting from each four-pointed star to the adhered end. Point 1 corresponds to a positive slope $\vartheta_1 > 0$, point 2 is for zero slope $\vartheta_2 = 0$, and point 3 corresponds to a negative slope $\vartheta_3 < 0$. The shape of the beam is described by the same Equation (8) but with different boundary conditions (no twisting is assumed for simplicity):

$$\begin{aligned} v(0) &= H_i, & v'(0) &= \vartheta_i; \\ v(s_i) &= 0, & v'(s_i) &= 0, \end{aligned} \tag{21}$$

where $i = 1, 2, 3$. The parameters entering here H_i , ϑ_i , and s_i are determined from the same experimental interferogram. Certainly, all three solutions are the parts of the same curve, but it is not that apparent that the adhesion energy is given by the same Equation (18) for the i th set of the parameters. In other words, is Equation (18) universal?

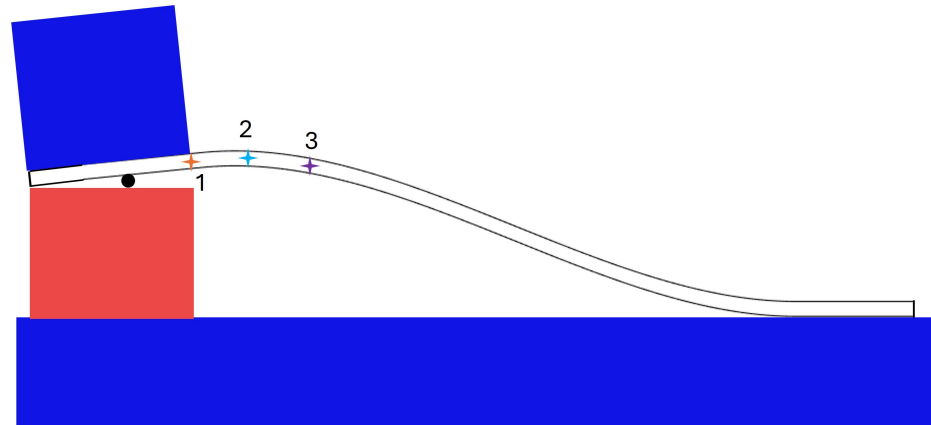


Figure 4. General case of the adhered cantilever. The experimental data are collected between locations 1, 2, or 3 and the adhered end.

To prove the universality, let the referent case be case 1: $H = H_1, s = s_1, \vartheta = \vartheta_1$. Then, from Equation (11), one finds the height H_i and the angle ϑ_i ($i \neq 1$):

$$\begin{aligned} H_i &= Hr^2 \left[-\gamma r^2 - (2 + a - 2\gamma)r + (3 + a - \gamma) \right], \\ \vartheta_i &= \frac{Hr}{s} \left[4\gamma r^2 + 3(2 + a - 2\gamma)r - 2(3 + a - \gamma) \right], \end{aligned} \tag{22}$$

where $r = s_i/s$. Using these relations, one can express the adhesion energy for the i th case via the parameters of case 1. After some transformations, one finds:

$$\Gamma_i = \Gamma_{0i} \left(1 - \frac{\gamma_i - a_i}{3} \right)^2 \equiv \Gamma_0 \left(1 - \frac{\gamma - a}{3} \right)^2, \tag{23}$$

where for the i th case, the parameters are

$$\Gamma_{0i} = \Gamma_0 \frac{H_i^2}{H^2 r^4}, \quad \gamma_i = \gamma \frac{H r^4}{H_i}, \quad a_i = \frac{\vartheta_i s_i}{H_i}.$$

The universality means that any segment of the bent cantilever that includes the adhered end can be used to determine the adhesion energy.

3. Interaction Energy

3.1. Parallel Plates

In the adhered area, the equilibrium distance between the surfaces in contact is $h_0 \gtrsim 10$ nm due to the roughness of microfabricated surfaces. If capillary forces can be excluded by the humidity control, only dispersion and electrostatic forces contribute to the interaction energy $\mathcal{W}(h_0)$. In the area of direct contact, additional surface forces can contribute, but this area is too small to significantly influence $\mathcal{W}(h_0)$, as was demonstrated previously [46,48].

Let $P(h)$ be the force per unit area acting between parallel flat plates. The interaction energy between parallel plates is

$$W(h) = \int_h^\infty dx P(x). \tag{24}$$

To calculate the interaction energy between rough surfaces $\mathcal{W}(h)$, one has to know the density distribution function $f(z)$, where z is the height of asperities with respect to the

average plane position of the rough surface. If $f(z)$ is known, then $\mathcal{W}(h_0)$ can be presented in the following form:

$$\mathcal{W}(h_0) \approx \int_{-\infty}^{h_0-h_c} dz f(z) W(h_0 - z), \tag{25}$$

where $h_c \approx 0.2$ nm is the smallest possible distance between the surfaces in contact due to short-range repulsion forces. Here, the approximate equality means the following. First, the contribution from the area of direct contact is neglected because the interaction energy at contact is about 0.1 J/m², but the relative area of direct contact is approximately of 10^{-6} . The resulting contribution to $\mathcal{W}(h_0)$ is then rather small, namely of about 0.1 μJ/m². Second, the exact value of h_c is determined by the balance of attractive and repulsive (elastic) forces, but if one takes $h_c = 0.2$ nm, the error $\mathcal{W}(h_0)$ is again of the order of 0.1 μJ/m². The exact form of Equation (25) is given in Ref. [46].

If one can neglect the contact contribution to the force, then only the dispersion and electrostatic forces are significant. The Casimir–Lifshitz force (or DF) is described in a general case by Lifshitz theory [2,3]. In this theory, the force cannot be presented analytically as a function of distance. For discussion purposes, let us use a simplified representation:

$$P_{CL}(h) = P_{CL}(h_0) \left(\frac{h_0}{h} \right)^\alpha. \tag{26}$$

Here, the exponent $3 < \alpha < 4$ is a slowly varying function of the distance h and can be treated as a constant within a finite range of distances. However, for all numerical calculations, the entire Lifshitz theory is employed.

An additional contribution to the total force $P(h)$ originates from the electrostatic force. Even if both contacting bodies are grounded, a residual potential difference exists due to the differences in the work functions of the materials. The electrostatic force acting between flat parallel plates is

$$P_{el}(h) = -\frac{\epsilon_0 V^2}{2h^2} \tag{27}$$

where ϵ_0 is the permittivity of the vacuum, and V is the potential difference between the contacting plates. The force here is chosen to be negative since it is attractive. A typical value for the potential difference is $V \sim 100$ mV.

For example, at $h_0 = 20$ nm, the DF between Si and Ru is $P_{CL}(h_0) = -1191$ Pa, and the exponent in the range near 20 nm is $\alpha = 3.30$. These values have been found using Lifshitz theory with the optical data in a wide range of frequencies taken from Ref. [49] for Ru and from Ref. [50] for Si. The force value can be compared with the electrostatic force at the same distance, that is, $P_{el}(h_0) = -111$ Pa, where the potential difference is taken to be $V = 100$ mV. This relation between the electrostatic and dispersion forces demonstrates a general tendency that the electrostatic force becomes less significant at a smaller separation compared to the distances $h \sim 100$ nm [8,10]. For the interaction energy between flat surfaces, it was found that $W_{CL}(h_0) = -9.86$ μJ/m² for the dispersion contribution and $W_{el}(h_0) = -2.21$ μJ/m² for the electrostatic one. The roughness effect makes increasing the magnitude of both these values (see below), but W_{CL} is affected more, as soon as it increases faster with a decreasing distance than W_{el} does.

The measured value of the adhesion energy Γ_{exp} determined according Equation (18) has to correspond to the theoretically predicted value: $\Gamma_{th} = -\mathcal{W}(h_0)$. The equality is realized at some average equilibrium distance between the surfaces h_0 . To stress is that one can use this relation in the opposite direction. Namely, it is possible to determine the unknown distance h_0 from the measured value $\Gamma_{exp} = \Gamma_{th}(h_0)$ as was proposed earlier [46,48].

3.2. Tilted Plates

Equation (18) defines the adhesion energy where the parameters ϑ , H , and s are determined from the measured shape $v(x)$. The value of Γ_{exp} measured in this way is expected be smaller than that from the theory because the adhered part can be tilted with

respect to the substrate. For a comparison between the theory and experiment, one has to take into account the theoretical calculations of the tilting angle due to twisting.

Let $\mathcal{W}(h)$ be the interaction energy per unit area between two rough parallel plates separated by the distance h . If there is a tilting angle between the plates $\varphi = \Delta v/w$, the effective energy between the plates can be calculated using Derjaguin's approximation [51] (proximity force approximation (PFA)). This approximation works well because the angle $\varphi \sim 10^{-4}$ is quite small. The effective interaction energy is

$$\mathcal{W}_{\text{eff}}(h_0) = \frac{1}{w} \int_{-w/2}^{w/2} dy \mathcal{W}(h_0 + \Delta v(1/2 + y/w)), \quad (28)$$

where h_0 is the equilibrium distance between the surfaces in contact. Since the adhesion energy is the work needed to separate the surfaces, one finds for the effective value that

$$\Gamma_{\text{eff}} = -\mathcal{W}_{\text{eff}}(h_0) = -\frac{1}{\Delta v} \int_{h_0}^{h_0 + \Delta v} dh \mathcal{W}(h). \quad (29)$$

If the energy between parallel plates $\mathcal{W}(h)$ is assumed to be known, then one can find the effective adhesion energy that can be compared with the experimental result defined by Equation (20).

4. Experimental Example

A scanning interferometer that is able to determine the shape of cantilevers with a precision of 1 nm has been demonstrated [42]. As a preliminary result, the shape of a Si microcantilever with a thickness of 10 μm , a length of 12 mm, and a width of 200 μm has been determined. In that study, the original interferogram was used to determine the adhesion energy between Si (cantilever) and Ru (substrate).

4.1. Determination of Γ_{exp}

The setup worked as follows. Two laser beams from the interferometer scan along the length of a cantilever, starting from the adhered end (see [42] for details). One beam moves on the substrate, while the other one goes on the edge of the cantilever. The centers of these two beams are separated by a distance of 35 μm . The reflected beams interfere and the resulting intensity is recorded as the signal. The signals are collected separately for the beams moving along the left or along the right edge of the cantilever.

The interferometer signal for the laser beams moving along the left side of the cantilever is shown in Figure 5a. The data between two red crosses are used to determine the shape of the cantilever from the interferogram. The position of the left cross, which is close to the fixed end, is chosen to exclude uncertainties in the signal that appear in the transition region at x close to zero. If one takes the initial point closer to the transition point, the error in the determination of the angle ϑ is considerably larger. The right cross indicates the last point taken at the inflection point. The red stars show the extrema of the interferogram. The blue dots in Figure 5b correspond to the height of the cantilever $h_0 + v(x, -w/2)$ restored from the data in Figure 5a. The restoration is unique because it is known that the function $v(x, -w/2)$ cannot have more than one maximum. The brown dots correspond to the height restored from the data collected from the scanning along the right side of the cantilever. These data correspond to the function $h_0 + v(x, +w/2)$. As one can see, the right side is not adhered and hangs above the substrate at a height of $h_0 + \Delta v$, demonstrating the effect of the twisting of the cantilever, where $\Delta v = 352$ nm.

The angle ϑ and the exact height H are determined from fitting the curve near the fixed end by a fourth-order polynomial. The exact value of the unadhered length s is determined from a similar fit at the adhered end. This procedure reduces the noise, which is the largest at both ends of the interferogram. The quality of the fits is demonstrated in the insets. In this way, it is found that $\vartheta = -0.223 \times 10^{-3}$, $H = 5.312$ μm , and $s = 9.978$ mm. Young's modu-

lus for a single crystal Si wafer with orientation (100) is $E = 169 \text{ GPa}$ [52]. Using a cantilever thickness of $t = 10 \text{ }\mu\text{m}$, one can find the following with the help of Equations (1) and (10):

$$\Gamma_0 = 0.72 \text{ }\mu\text{J}/\text{m}^2, a = -0.419, \gamma = 1.262, b = 0.066, \tag{30}$$

where the silicon mass density $\rho = 2.33 \times 10^3 \text{ kg}/\text{m}^3$ has been taken. As one can see, the parameters a and γ cannot be neglected in Equation (20). Using these parameters, one can find the experimental value of the adhesion energy $\Gamma_{\text{exp}} = 0.11 \text{ }\mu\text{J}/\text{m}^2$. The errors on Γ are not discussed here in detail, but they cannot be larger than 5%, as statistical analysis demonstrates. The adhesion energy is unexpectedly small. The reason for such a small value is related to the twisting of the cantilever and the significant roughness of the interacting surfaces.

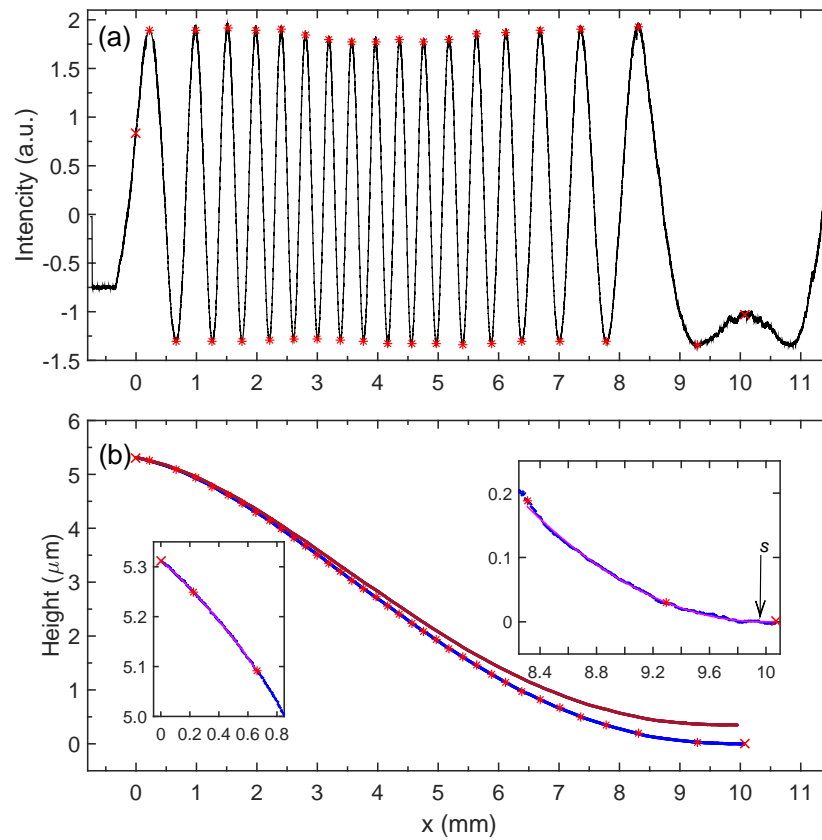


Figure 5. (a) Intensity signal recorded for two laser beams moving along the left side of the cantilever. The red stars show the extrema positions, and the crosses indicate the first and the last point used in calculations. (b) The shape of the adhered cantilever extracted from the interference signal as a function of the x -coordinate. Blue dots present the data collected for the beams moving along the left side, and brown dots are those for the right side. The inset on the left shows a zoomed-in view near the fixed end. The inset on the right demonstrates the data near the adhered end. The magenta curves fit the noisy data near the ends.

Figure 6a shows the height difference $v_R - v_L$ between the right and left sides of the cantilever as a function of x . It confirms the linear dependence that has been assumed in Equation (13). Quite close to the adhesion point, the transition to a constant value occurs as it should be for the adhered part. Since the transition region is narrow, a sharp transition was assumed in Section 2.2.2 that resulted in boundary conditions (14). The adhesion energy (16) can obtain an additional correction if the forces acting in the adhered region contribute to the twisting. If in the adhered area, only the DF is involved, it produces the following moment of force:

$$\begin{aligned}
 M_{DF} &= (L - s) \int_0^w P_{CL}(h_0 + v(s, l - w/2)) l dl \\
 &= (L - s) w^2 P_{CL}(h_0) I(\Delta v/h_0),
 \end{aligned}
 \tag{31}$$

where $I(q)$ is defined as

$$I(q) = \int_0^1 (1 + qx)^{-\alpha} x dx.
 \tag{32}$$

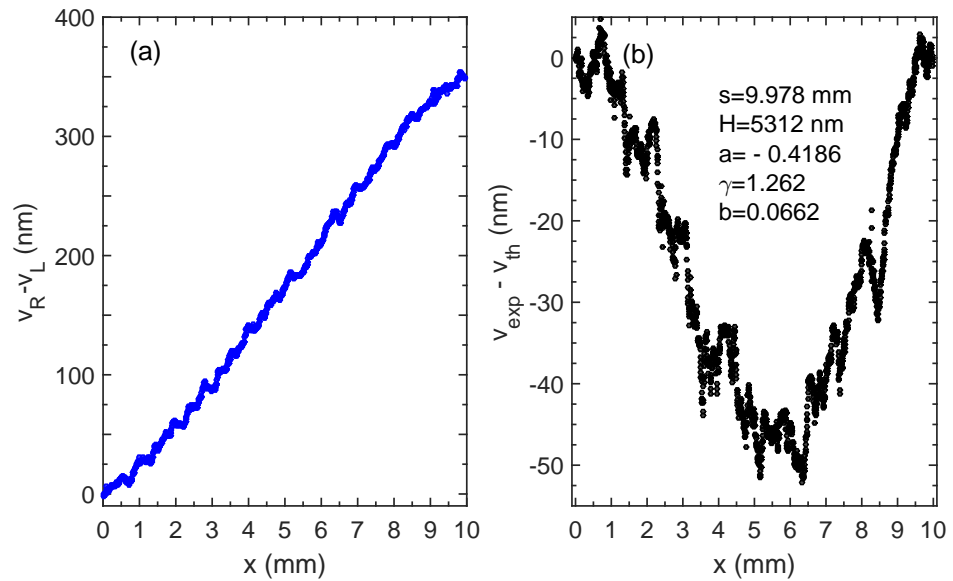


Figure 6. (a) The height difference between the right and the left side of the cantilever as a function of distance x . (b) Difference between the shapes measured experimentally and predicted theoretically. The agreement is good since the deviation is not more than 1%.

Here, the simplified form (26) of the DF is used to estimate the force. From the mechanical point of view, the moment M_{DF} results in the twisting of the beam on the angle $\varphi_{DF} = \Delta v_{DF}/w$ according to the equation [53]: $M_{DF} = 0.333 t^3 G \varphi_{DF}$, where $G = 79.4$ GPa is the shear modulus of (100) Si [54]. If the ratio $\Delta v_{DF}/\Delta v \ll 1$, the beam twisting is the built-in effect, and twisting does not contribute to the energy (16). Calculations demonstrate that the ratio $\Delta v_{DF}/\Delta v$ decreases from 0.26 at $h_0 = 10$ nm to 0.026 at $h_0 = 50$ nm. In the specific example considered here, the value of h_0 is estimated (see below) as 45 nm, which gives $\Delta v_{DF}/\Delta v = 0.031$. Therefore, the twisting can be neglected in the energy.

It is also necessary to see how good the measured shape of the cantilever is described by the theoretical curve (11). The difference between the experimental and theoretical curves $v_{exp} - v_{th}$ as a function of x is shown in Figure 6b. One can see that the deviation is negative as it should be if some external attractive force like dispersion or electrostatic force is acting outside of the adhered area. The magnitude of the deviation is about 1% of the height H in its maximum. The position of the maximum is shifted to the adhered end. All these features have to be observed if the DF is acting between the cantilever and the substrate outside of the adhered area [41]. However, it is too early to state that the observed deviation is due to the DF. More theoretical and experimental studies need to be done to support the statement.

4.2. Roughness

The roughness of the contacting surfaces is essential for the theoretical prediction of the adhesion energy. Although the working surface of the cantilever is the polished side of the SOI wafer, it becomes rough after oxidation with the following etching of the oxide. The substrate is covered by a deposited material, which in this case is ruthenium. The AFM

scans of both surfaces have been presented in Ref. [42]. The scanned area was $5 \times 5 \mu\text{m}^2$, recorded with a resolution of 1024 pixels per line. For each surface, three scans recorded in different places have been performed. The roughness of both surfaces cannot be described by the normal distribution, as one can see in Figure 7a,b. The deviation is well visible on the logarithmic vertical scale. There are much more high peaks than those predicted by the normal distribution. This effect was already stressed previously for the magnetron [55] deposition of metals on a cold substrate without annealing.

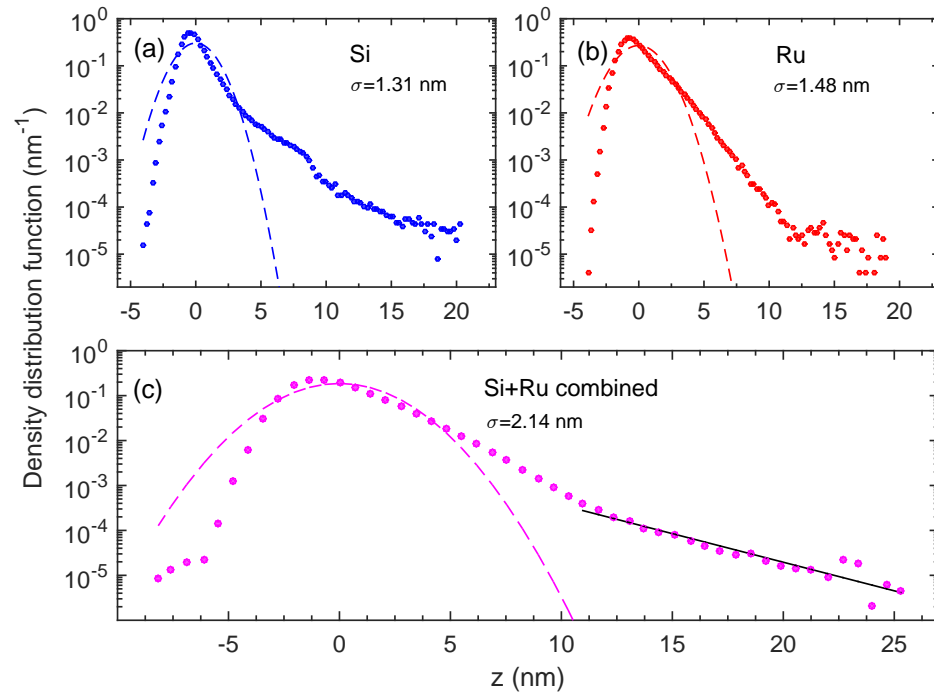


Figure 7. Density distribution function for asperity heights z . (a) Working face of the cantilever (Si). The dashed curve shows the normal distribution with the same RMS roughness σ . (b) The same for the substrate covered by sputtered Ru. (c) The distribution function $f(z)$ for the combined image (Si+Ru) averaged over nine different combination AFM scans. The solid line is the linear fit of $\ln f(z)$ at large z . See text for details.

The interaction energy between two rough surfaces is equivalent to the interaction between a flat surface and a rough surface with a combined roughness, which can be presented as a sum of two AFM scans. The density distribution function shown in Figure 7c is the average distribution function found from the different combined scans of the substrate and the cantilever (nine combinations in total). Although the root mean square (RMS) roughness is not large, $\sigma = 2.14 \pm 0.14 \text{ nm}$, exceptionally high peaks up to 25 nm can be found on an area of $5 \times 5 \mu\text{m}^2$. At $z > 5\sigma$, the curve can be described by the exponent $Be^{-z/\Sigma}$, as the solid black line demonstrates, where $B = 6.87 \times 10^{-3} \text{ nm}^{-1}$ and $\Sigma = 3.41 \text{ nm}$ are the parameters. Note that Σ is larger than the RMS roughness ($\sigma = 2.14 \text{ nm}$). This kind of distribution has been observed previously, for example, for magnetron sputtered Cu [55]. The asymptotic behavior of $f(z)$ is essential to relate the distance on contact h_0 with the interaction energy according to Equation (25).

4.3. Relation Between Γ and h_0

If the distribution function $f(z)$ is known, one can calculate the adhesion energy $\Gamma_{\text{th}}(h_0) = -\mathcal{W}(h_0)$. The result is shown in Figure 8a, where the solid blue curve shows the contribution of the DF in Γ , and the gray stripe demonstrates uncertainty due to the electrostatic interaction with $V \leq 100 \text{ mV}$. However, it is not possible to compare this curve directly with the experimental result $\Gamma_{\text{exp}} = 0.11 \mu\text{J}/\text{m}^2$ because the cantilever is twisted. Instead, the effective value Γ_{eff} given by Equation (29) has to be compared with

Γ_{exp} . The effective adhesion energy for pure dispersion interaction as a function of contact distance h_0 is shown in Figure 8b, where again the gray stripe demonstrates the uncertainty due to the electrostatic interaction. For the effective energy, the electrostatic interaction is crucial as soon as it decays slower with the increasing distance. The measured value of the adhesion energy is shown by the thick horizontal dashed line.

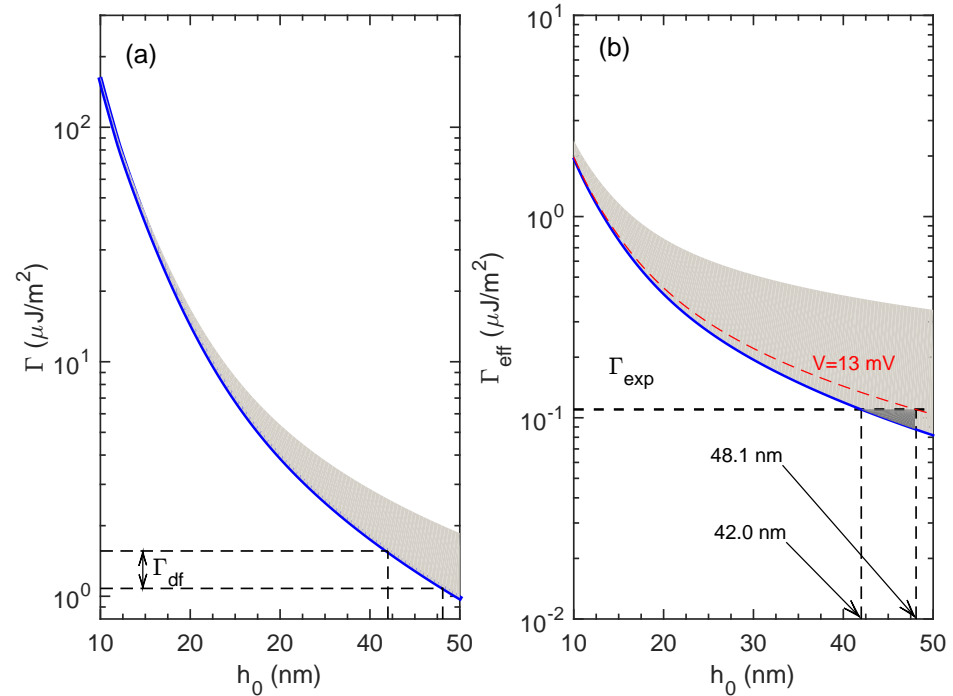


Figure 8. (a) Calculated value of the adhesion energy Γ as a function of contact distance h_0 . The blue curve corresponds to pure dispersion interaction, but the gray stripe shows possible uncertainty due to the electrostatic interaction with the potential difference $V < 100$ mV. The true value of the adhesion energy due to pure dispersion interaction lies between the horizontal dashed lines. (b) The same but for the effective adhesion energy Γ_{eff} that takes into account the twisting of the cantilever. The thick dashed line corresponds to the measured adhesion energy Γ_{exp} that has to be compared with Γ_{eff} . The dark-gray curved triangle demonstrates the allowed region of the parameters, that is, $42.0 < h_0 < 48.1$ nm and $V < 13$ mV. See text for details.

The position of the cross-point between the dashed line and solid curve gives the equilibrium value of the distance on contact $h_0 = 42.0$ nm. This value has to be considered as the lower limit on the equilibrium distance because it corresponds to the minimum potential difference $V = 0$. On the other hand, one can find the absolute upper limit for h_0 . The adhered part of the cantilever has to make contact with the substrate in at least three points. The total number of pixels in the nominal adhered area is $N = (L - s)w / A_{\text{px}} \approx 1.68 \times 10^{10}$, where $A_{\text{px}} = (5000 \text{ nm} / 1024)^2 = 23.8 \text{ nm}^2$ is the area of one pixel. The relative area of direct contact that takes into account the twisting angle $\varphi = \Delta v / w$ is

$$R(h_0) = \frac{1}{w} \int_{-w/2}^{w/2} dy \int_{z_0(y)}^{\infty} dz f(z), \tag{33}$$

where $z_0(y) = h_0 - h_c + \Delta v(1/2 + y/w)$ is the local height. In using the asymptotic presentation for $f(z) = B e^{-z/\Sigma}$ at $z > 5w$, the contact area is

$$R(h_0) \approx \frac{\Sigma^2 B}{\Delta v} e^{-(h_0 - h_c)/\Sigma}. \tag{34}$$

From the condition $NR(h_0) > 3$, one finds the upper limit $h_0 < 48.1$ nm; thus, the contact distance has to be in the interval $42.0 < h_0 < 48.1$ nm. Indeed, at exceptionally

large z , the distribution function can decrease faster, but 48.1 nm can be taken as the absolute upper limit.

The dark-gray curved triangle in Figure 8b demonstrates the allowed region of the parameters in the (h_0-V) space. The red dashed curve shows that the allowed potential difference is not more than 13 mV. The value of the adhesion energy Γ_{DF} related to pure dispersion interaction is between the ordinates of the blue curve in Figure 8a corresponding to the interval $42.0 < h_0 < 48.1$ nm. The value of Γ_{DF} lies in the interval $1.09 < \Gamma_{DF} < 1.56 \mu\text{J}/\text{m}^2$.

4.4. Discussion

The analysis of the experimental example allows us to make several conclusions, which are significant for actual experiments with adhered cantilevers. First, there is a technological problem related to the twisting of the cantilever. It strongly reduces the measured value Γ_{exp} and introduces uncertainties in the true value of the adhesion energy Γ . Still, there is no complete understanding about the factors driving the twisting. The second critical issue is the significant roughness of the interacting surfaces. It defines the minimal distance between the surfaces in contact h_0 . The adhered cantilever method is designed for $h_0 \sim 10$ nm, but in the example in Section 4.3, it is found to exceed 40 nm. For larger h_0 , the DFs become weaker and the effect of the electrostatic forces is relatively stronger. The crucial parameter in this case is not the RMS roughness but the excessive number of high peaks in the distribution function. For the substrate covered with a metal, the issue, however, is not of high importance. Indeed, one can sputter the metal on a hot substrate to obtain normal distribution [55]. However, the roughness of the working surface of the cantilever will stay significant. This effect is due to the fabrication steps related to the oxidation of the SOI wafer with the following etching of the oxide. One has to look for methods to reduce the roughness or even change the fabrication method for cantilevers.

From Figure 8b, one can conclude that at larger h_0 , the role of the electrostatic interaction increases. In all experiments where the Casimir–Lifshitz force has been measured, the electrostatic force was minimized by applying a compensating potential. For the adhered cantilever method, the effect of the electrostatic force is less critical but still necessary to be minimized. This can be included in the technological process. If the electrostatic interaction can be minimized, then, from Figure 8b, one can find a precise value of h_0 and, from Figure 8a, the true value of the adhesion energy induced by the DF.

On the other hand, the adhered cantilever method is highly attractive. The method can be applied to different materials. The nominal interaction area is large in comparison with all the other Casimir-type experiments, and for this reason, one may deal with much stronger forces. Surely, the main advantage of the method is the possibility to measure the dispersion interaction at quite short separations without the loss of stability.

5. Conclusions

This paper is devoted to the development of a new method to measure the Casimir–Lifshitz forces or, more generally, the dispersion forces at distances in the order of 10 nm. Standard methods to measure these forces fail at short separations due to loss of stability. The adhered cantilever method is stable at any separation distance and can measure the forces directly at the contact distance. To obtain information on the acting forces, one has to know the precise shape of the cantilever in a considerably wide range of heights. An interferometric setup that is able to collect this information has been presented recently [42]. The first application of the setup to minicantilevers produced using microfabrication methods revealed a number of nonidealities that do not allow one to use the standard relation (1) between the adhesion energy and the parameters of the cantilever.

A new relation for the adhesion energy (20) is deduced in this paper and can be used for slightly twisted cantilevers that have a nonzero angle at the fixed end and are subject to gravity. The effects of nonideality significantly change the value of the adhesion energy compared to the generally accepted relation (1).

The new relation is applied to the first test result from the setup where a silicon cantilever adhered to a substrate sputtered with ruthenium. The analysis of the data revealed a significant role of the roughness of the surfaces in contact. An essential deviation in high asperities from the normal distribution and large nominal contact area provide a rather large contact distance in the range of 45 nm. Although the effect of the electrostatic potential difference between the surfaces is not significant, the importance of unknown electrostatics increases due to the twisting of the cantilever. The twisting also reduces the measured adhesion energy to a small value of $\Gamma_{\text{exp}} = 0.11 \mu\text{J}/\text{m}^2$ as soon as only one side of the cantilever is adhered and the other side hangs above the substrate. The recalculated value corresponding to the parallel surfaces gives a true adhesion energy of $1.3 \mu\text{J}/\text{m}^2$ with uncertainty defined by the electrostatic contribution.

The analysis performed demonstrated some possible issues of the setup to be addressed before carrying out the measurements.

Author Contributions: Conceptualization, I.A.S. and V.B.S.; methodology, I.A.S. and V.B.S.; validation, I.A.S. and V.B.S.; investigation, I.A.S. and V.B.S.; resources, V.B.S.; data curation, V.B.S.; writing—original draft preparation, V.B.S.; writing—review and editing, I.A.S.; funding acquisition, V.B.S. All authors have read and agreed to the published version of the manuscript.

Funding: This work is supported by the Russian Science Foundation, Grant No. 24-29-00106.

Data Availability Statement: Data are contained within the article.

Conflicts of Interest: The authors declare no conflicts of interest.

References

1. Casimir, H.B.G. On the attraction between two perfectly conducting plates. *Proc. Kon. Ned. Akad. Wetensch. B* **1948**, *51*, 793–795. Available online: <https://dwc.knaw.nl/DL/publications/PU00018547.pdf> (accessed on 10 October 2024).
2. Lifshitz, E.M. The theory of molecular attractive forces between solids. *Sov. Phys. JETP* **1956**, *2*, 73–83. Available online: <http://jetp.ras.ru/cgi-bin/e/index/e/2/1/p73?a=list> (accessed on 10 October 2024).
3. Dzyaloshinskii, I.E.; Lifshitz, E.M.; Pitaevskii, L.P. General theory of van der Waals' forces. *Sov. Phys. Uspekhi* **1961**, *4*, 153–176. [[CrossRef](#)]
4. Klimchitskaya, G.L.; Mohideen, U.; Mostepanenko, V.M. The Casimir force between real materials: Experiment and theory. *Rev. Mod. Phys.* **2009**, *81*, 1827–1885. [[CrossRef](#)]
5. Rodriguez, A.W.; Capasso, F.; Johnson, S.G. The Casimir effect in microstructured geometries. *Nat. Photonics* **2011**, *3*, 211–221. [[CrossRef](#)]
6. Palasantzas, G.; Sedighi, M.; Svetovoy, V.B. Applications of Casimir forces: Nanoscale actuation and adhesion. *Appl. Phys. Lett.* **2020**, *117*, 120501. [[CrossRef](#)]
7. Lamoreaux, S.K. Demonstration of the Casimir force in the 0.6 to 6 μm range. *Phys. Rev. Lett.* **1997**, *78*, 5–8. [[CrossRef](#)]
8. Harris, B.W.; Chen, F.; Mohideen, U. Precision measurement of the Casimir force using gold surfaces. *Phys. Rev. A* **2000**, *62*, 052109. [[CrossRef](#)]
9. Chan, H.B.; Aksyuk, V.A.; Kleiman, R.N.; Bishop, D.J.; Capasso, F. Quantum mechanical actuation of microelectromechanical systems by the Casimir force. *Science* **2001**, *291*, 1941–1944. [[CrossRef](#)]
10. Decca, R.S.; López, D.; Fischbach, E.; Krause, D.E. Measurement of the Casimir force between dissimilar metals. *Phys. Rev. Lett.* **2003**, *91*, 050402. [[CrossRef](#)]
11. Bressi, G.; Carugno, G.; Onofrio, R.; Ruoso, G. Measurement of the Casimir force between parallel metallic surfaces. *Phys. Rev. Lett.* **2002**, *88*, 041804. [[CrossRef](#)] [[PubMed](#)]
12. Decca, R.; López, D.; Fischbach, E.; Klimchitskaya, G.; Krause, D.; Mostepanenko, V. Precise comparison of theory and new experiment for the Casimir force leads to stronger constraints on thermal quantum effects and long-range interactions. *Ann. Phys. (N. Y.)* **2005**, *318*, 37–80. [[CrossRef](#)]
13. London, F. Zur Theorie und Systematik der Molekularkräfte. *Z. Phys.* **1930**, *63*, 245–279. [[CrossRef](#)]
14. Liu, M.; Xu, J.; Klimchitskaya, G.L.; Mostepanenko, V.M.; Mohideen, U. Precision measurements of the gradient of the Casimir force between ultraclean metallic surfaces at larger separations. *Phys. Rev. A* **2019**, *100*, 052511. [[CrossRef](#)]
15. Bimonte, G.; Spreng, B.; Maia Neto, P.A.; Ingold, G.L.; Klimchitskaya, G.L.; Mostepanenko, V.M.; Decca, R.S. Measurement of the Casimir force between 0.2 and 8 μm : Experimental procedures and comparison with theory. *Universe* **2021**, *7*, 93. [[CrossRef](#)]
16. Tonck, A.; Houzé, F.; Boyer, L.; Loubet, J.-L.; Georges, J.-M. Electrical and mechanical contact between rough gold surfaces in air. *J. Phys. Cond. Matt.* **1991**, *3*, 5195–5201. [[CrossRef](#)]
17. van Zwol, P.J.; Palasantzas, G.; van de Schootbrugge, M.; De Hosson, J.T.M. Measurement of dispersive forces between evaporated metal surfaces in the range below 100nm. *Appl. Phys. Lett.* **2008**, *92*, 054101. [[CrossRef](#)]

18. Torricelli, G.; van Zwol, P.J.; Shpak, O.; Binns, C.; Palasantzas, G.; Kooi, B.J.; Svetovoy, V.B.; Wuttig, M. Switching Casimir forces with phase-change materials. *Phys. Rev. A* **2010**, *82*, 010101. [[CrossRef](#)]
19. Sedighi, M.; Svetovoy, V.B.; Palasantzas, G. Casimir force measurements from silicon carbide surfaces. *Phys. Rev. B* **2016**, *93*, 085434. [[CrossRef](#)]
20. DelRio, F.W.; de Boer, M.P.; Knapp, J.A.; Reedy, E.D.; Clews, P.J.; Dunn, M.L. The role of van der Waals forces in adhesion of micromachined surfaces. *Nat. Mater.* **2005**, *4*, 629–634. [[CrossRef](#)]
21. Hariri, A.; Zu, J.W.; Mrad, R.B. Modeling of dry stiction in micro electro-mechanical systems (MEMS). *J. Micromech. Microeng.* **2006**, *16*, 1195. [[CrossRef](#)]
22. Xue, X.; Polycarpou, A.A.; Phinney, L.M. Measurement and modeling of adhesion energy between two rough microelectromechanical system (MEMS) surfaces. *J. Adhes. Sci. Technol.* **2008**, *22*, 429–455. [[CrossRef](#)]
23. Pastewka, L.; Robbins, M.O. Contact between rough surfaces and a criterion for macroscopic adhesion. *Proc. Natl. Acad. Sci. USA* **2014**, *111*, 3298–3303. [[CrossRef](#)] [[PubMed](#)]
24. Parsons, D.F.; Walsh, R.B.; Craig, V.S.J. Surface forces: Surface roughness in theory and experiment. *J. Chem. Phys.* **2014**, *140*, 164701. [[CrossRef](#)] [[PubMed](#)]
25. Svetovoy, V.B.; Postnikov, A.V.; Uvarov, I.V.; Stepanov, F.I.; Palasantzas, G. Measuring the dispersion forces near the van der Waals–Casimir transition. *Phys. Rev. Appl.* **2020**, *13*, 064057. [[CrossRef](#)]
26. Legtenberg, R.; Tilmans, H.A.; Elders, J.; Elwenspoek, M. Stiction of surface micromachined structures after rinsing and drying: Model and investigation of adhesion mechanisms. *Sens. Actuators A Phys.* **1994**, *43*, 230–238. [[CrossRef](#)]
27. Tas, N.; Sonnenberg, T.; Jansen, H.; Legtenberg, R.; Elwenspoek, M. Stiction in surface micromachining. *J. Micromech. Microeng.* **1996**, *6*, 385–397. [[CrossRef](#)]
28. Man, P.; Gogoi, B.; Mastrangelo, C. Elimination of post-release adhesion in microstructures using conformal fluorocarbon coatings. *J. Microelectromech. Syst.* **1997**, *6*, 25–34. [[CrossRef](#)]
29. Maboudian, R.; Ashurst, W.; Carraro, C. Self-assembled monolayers as anti-stiction coatings for MEMS: characteristics and recent developments. *Sens. Actuators A Phys.* **2000**, *82*, 219–223. [[CrossRef](#)]
30. Ashurst, W.; Carraro, C.; Maboudian, R.; Frey, W. Wafer level anti-stiction coatings for MEMS. *Sens. Actuators A Phys.* **2003**, *104*, 213–221. [[CrossRef](#)]
31. Romig, A.; Dugger, M.T.; McWhorter, P.J. Materials issues in microelectromechanical devices: Science, engineering, manufacturability and reliability. *Acta Mater.* **2003**, *51*, 5837–5866. [[CrossRef](#)]
32. Mastrangelo, C.H.; Hsu, C.H. Mechanical stability and adhesion of microstructures under capillary forces. I. Basic theory. *J. Microelectromech. Syst.* **1993**, *2*, 33–43. [[CrossRef](#)]
33. Mastrangelo, C.H.; Hsu, C.H. Mechanical stability and adhesion of microstructures under capillary forces. II. Experiments. *J. Microelectromech. Syst.* **1993**, *2*, 44–55. [[CrossRef](#)]
34. Maboudian, R.; Howe, R.T. Critical Review: Adhesion in surface micromechanical structures. *J. Vac. Sci. Technol. B* **1997**, *15*, 1–20. [[CrossRef](#)]
35. Parker, E.E.; Ashurst, W.R.; Carraro, C.; Maboudian, R. Adhesion characteristics of MEMS in microfluidic environments. *J. Microelectromech. Syst.* **2005**, *14*, 947–953. [[CrossRef](#)]
36. de Boer, M.P.; Michalske, T.A. Accurate method for determining adhesion of cantilever beams. *J. Appl. Phys.* **1999**, *86*, 817–827. [[CrossRef](#)]
37. Knapp, J.A.; de Boer, M.P. Mechanics of microcantilever beams subject to combined electrostatic and adhesive forces. *J. Microelectromech. Syst.* **2002**, *11*, 754–764. [[CrossRef](#)]
38. Zhang, Y.; Zhao, Y.-p. A precise model for the shape of an adhered microcantilever. *Sens. Actuators A Phys.* **2011**, *171*, 381–390. [[CrossRef](#)]
39. Zhang, Y.; Zhao, Y.-p. Flexural contact in MEMS stiction. *Int. J. Solids Struct.* **2012**, *49*, 2203–2214. [[CrossRef](#)]
40. Mastrangelo, C.H.; Hsu, C.H. A simple experimental technique for the measurement of the work of adhesion of microstructures. In Proceedings of the Technical Digest IEEE Solid-State Sensor and Actuator Workshop, Hilton Head Island, SC, USA, 22–25 June 1992; Institut of Electrical and Electronics Engineers (IEEE): New York, NY, USA, 1992; pp. 208–212. [[CrossRef](#)]
41. Svetovoy, V.B.; Melenev, A.E.; Lokhanin, M.V.; Palasantzas, G. Global consequences of a local Casimir force: Adhered cantilever. *App. Phys. Lett.* **2017**, *111*, 011603. [[CrossRef](#)]
42. Postnikov, A.V.; Uvarov, I.V.; Svetovoy, V.B. Experimental setup for measuring the dispersion forces by the adhered cantilever method. *Rev. Sci. Instrum.* **2023**, *94*, 043907. [[CrossRef](#)] [[PubMed](#)]
43. Lang, W. Nomarski differential interference-contrast microscopy. *Zeiss Inf.* **1968**, *70*, 114–120. Available online: <https://zeiss-campus.magnet.fsu.edu/referencelibrary/abstracts/dic01.html> (accessed on 10 October 2024).
44. Jensen, B.; de Boer, M.; Masters, N.; Bitsie, F.; LaVan, D. Interferometry of actuated microcantilevers to determine material properties and test structure nonidealities in MEMS. *J. Microelectromech. Syst.* **2001**, *10*, 336–346. [[CrossRef](#)]
45. Soylemez, E.; de Boer, M.P. Van der Waals force-induced crack healing in dry rough interfaces. *J. Phys. D* **2016**, *49*, 075303. [[CrossRef](#)]
46. Soldatenkov, I.A.; Stepanov, F.I.; Svetovoy, V.B. Dispersion forces and equilibrium distance between deposited rough films in contact. *Phys. Rev. B* **2022**, *105*, 075401. [[CrossRef](#)]

47. Svetovoy, V.B.; Soldatenkov, I.A. Weak adhesion between contacting rough surfaces as applied to micro/nanotechnologies. *Colloid J.* **2022**, *84*, 321–331. [[CrossRef](#)]
48. Soldatenkov, I.A.; Palasantzas, G.; Svetovoy, V.B. Weak adhesion between deposited rough films: Relation to the dispersion forces. *Phys. Rev. B* **2021**, *104*, L121404. [[CrossRef](#)]
49. Babamahdi, Z.; Svetovoy, V.B.; Enache, M.; Stöhr, M.; Palasantzas, G. Comparison of Casimir forces and electrostatics from conductive SiC-Si/C and Ru surfaces. *Phys. Rev. B* **2019**, *100*, 245422. [[CrossRef](#)]
50. Palik, E.D. (Ed.) *Handbook of Optical Constants of Solids*; Academic Press, Inc.: San Diego, CA, USA, 1985. [[CrossRef](#)]
51. Derjaguin, B. Untersuchungen über die Reibung und Adhäsion, IV. Theorie des Anhaftens kleiner Teilchen. *Koll.-Zeitsch.* **1934**, *69*, 155–164. [[CrossRef](#)]
52. Hopcroft, M.A.; Nix, W.D.; Kenny, T.W. What is the Young's modulus of silicon? *J. Microelectromech. Syst.* **2010**, *19*, 229–238. [[CrossRef](#)]
53. Feodosyev, V. *Strength of Materials*; Mir Publishers: Moscow, Russia, 1968.
54. Kim, J.; Cho, D.-i.; Muller, R.S. Why is (111) silicon a better mechanical material for MEMS? In *Transducers '01 Eurosensors XV*; Obermeier, E., Ed.; Springer: Berlin/Heidelberg, Germany, 2001; pp. 662–665. [[CrossRef](#)]
55. Muravyeva, T.I.; Uvarov, I.V.; Naumov, V.V.; Palasantzas, G.; Svetovoy, V.B. Excessive number of high asperities for sputtered rough films. *Phys. Rev. B* **2021**, *104*, 035415. [[CrossRef](#)]

Disclaimer/Publisher's Note: The statements, opinions and data contained in all publications are solely those of the individual author(s) and contributor(s) and not of MDPI and/or the editor(s). MDPI and/or the editor(s) disclaim responsibility for any injury to people or property resulting from any ideas, methods, instructions or products referred to in the content.